energies

Article

Corner Separation Control Using a New Combined Slotted Configuration in a High-Turning Compressor Cascade under Different Solidities

Hejian Wang [1], Yanshan Qing [2], Bo Liu [1,*] and Xiaochen Mao [1]

[1] School of Power and Energy, Northwestern Polytechnical University, 1 Dongxiang Road, Chang'an District, Xi'an 710129, China; hejian_wang@mail.nwpu.edu.cn (H.W.); maoxiao_chen@nwpu.edu.cn (X.M.)
[2] Chinese People's Liberation Army, No. 5719 Factory, 91 Baihe Road, Lichun District, Pengzhou 611936, China; yanshan_qing@126.com
* Correspondence: liubo704@nwpu.edu.cn

Abstract: In order to comprehensively control the corner separation and the blade trailing edge (TE) separation in a high-turning compressor stator cascade, this research proposes a new combined slotted configuration consisting of one full-span slot and two blade-end slots. Taking into account the effect of the blade solidity, the performance of the original cascade and the combined slotted cascade was calculated and evaluated in a wide incidence angle range at two blade solidities. The results indicated that the blade loading and the corner separation range of the original cascade becomes larger as the blade solidity decreases from 1.66 to 1.36, which leads to higher total pressure loss and lower pressure diffusing capacity under positive incidence angles. The low-momentum fluid in the boundary layer can be significantly re-energized by the high-momentum blade-end and full-span slots jets, hence the combined slotted configuration can eliminate the blade TE separation and reduce the corner separation remarkably in the full incidence angle range at the two blade solidities. By adopting the combined slotted configuration, the total pressure loss, turning angle and static pressure coefficient of the original cascade can be increased by −23.2%, 2.7° and 4.7% on average, respectively, when the blade solidity is 1.66, while they can be increased by −27.7%, 3.3° and 7.6% on average, respectively, when the blade solidity is 1.36. The combined slotted configuration has a significant adaptability to the low blade solidity (or high loading) condition and it shows a certain potential in increasing the aeroengine thrust-to-weight ratio by decreasing the compressor single-stage blade number.

Keywords: high-turning compressor stator cascade; full-span slot; blade-end slot; corner separation; pressure diffusing capacity; low blade solidity; aeroengine thrust-to-weight ratio

Citation: Wang, H.; Qing, Y.; Liu, B.; Mao, X. Corner Separation Control Using a New Combined Slotted Configuration in a High-Turning Compressor Cascade under Different Solidities. *Energies* **2021**, *14*, 3376. https://doi.org/10.3390/en14123376

Academic Editor: Galih Bangga

Received: 26 April 2021
Accepted: 7 June 2021
Published: 8 June 2021

1. Introduction

The axial compressor is the core component of aero-engines and it has a great impact on the aero-engines performance [1]. As an inherent flow phenomenon in compressors [2], three-dimensional (3D) corner separation may cause serious total pressure loss and passage blockage with the increase in blade loading [3]. Therefore, the flow mechanism of 3D corner separation has been widely investigated by scholars by using experimental methods [4], Reynolds-averaged Navier-Stokes (RANS) method [5,6], large-eddy simulation (LES) method [7,8] and delayed detached eddy simulation (DDES) method [9,10].

According to the previous studies, under the strong adverse pressure gradient along the mainstream direction, 3D corner separation is always produced due to the interference of the end-wall boundary layer and the blade boundary layer. Additionally, under the pressure gradient substantially perpendicular to the mainstream direction, the low-momentum fluid will be transported into the hub-corner region by the significant cross-passage flow. Hence, as the blade turning or loading increases, the end-wall (EW) low-momentum fluid starts to migrate to the blade suction surface (SS) sooner, which will cause the 3D corner separation to become more serious. Based on Denton's establishing, about one-third of the losses in axial compressors are the secondary flow losses in the hub-corner region [11]. Therefore, 3D corner separation has a significant impact on the performance of compressors. In order to enhance the working stability and efficiency of compressors, it is important to do so by controlling and alleviating 3D corner separation [12].

Internal flow control methods have a significant potential in controlling 3D corner separation [13]. The low-momentum fluid in the boundary layer can be aspirated by the suction slot, thus effectively suppressing flow separation. In the studies of Ankit et al. [14] and Mao [15], the corner separation was significantly controlled using boundary layer suction, contributing to a broadening of available incidence angle range and an improvement of pressure diffusing capacity. In the study of Qin et al. [16], the EW jet flow was used to control 3D corner separation. The results showed that the total pressure loss and static pressure rise coefficient can be respectively increased by up to −7.3% and 3.3%. Moreover, Liu et al. [17] applied an EW vortex generator in a high-turning compressor cascade, achieving a significant loss reduction in a wide incidence angle range. Zhao et al. [18] studied the impact of partial clearance on the performance of a 1.5-stage axial compressor, discovering that the stability margin of the compressor can be enlarged in the suitable partial clearance case. Additionally, other methods such as blade curving [19], non-axisymmetric EW profiling [20], tandem blades [21], etc., are also beneficial for controlling 3D corner separation.

With the exception of the flow control methods mentioned above, blade slotting was widely used to control 3D corner separation as well. Tang et al. [22] applied slot structure at the end of a low solidity compressor cascade. Under the blowing of the blade-end slot jet, the passage vortex (P_V) and concentrated shedding vortex (CS_V) were reduced remarkably and the operating incidence angle range was broadened from $-8°$–$-4°$ to $-8°$–$4°$. Hu et al. [23] combined a full-span slot and EW vortex generator in a compressor stator cascade. Under the combined control effect of the vortex generated by the generator and the full-span slot jet, the corner separation was alleviated remarkably and the total pressure loss could be reduced by an average of 30.9%.

For the compressor design, blade solidity (chord-pitch ratio: c/t) was identified as an important parameter by Zweifel et al. [24] and Lieblein et al. [25] since it had a great effect on the blade loading and available incidence angle range. By keeping the blade chord length (c) constant, generally, the decrease in blade solidity will lead to higher blade loading and a larger separation zone. Sans et al. [26] investigated the blade solidity effect on the cascade performance at a numerically high Mach number condition. The study concluded that under large positive incidence angles, the smaller solidity cascade experiences more loss as compared to the higher solidity cascade. This is because smaller blade solidity brings higher blade loading, thus decreasing the cascade stability range.

Blade slotting shows a certain potential in controlling 3D corner separation [22,23,27], but most of the previous studies about slotted blades investigated the front-loaded blade profile. In this research, a high-turning compressor stator cascade with a post-loaded blade profile was selected as the research object. To comprehensively control the corner separation and the TE separation, two blade-end slots and one full-span slot were combined in the cascade. Afterwards, in order to check the suitability of the combined slotted configuration for higher loading or larger separation conditions, the blade solidity of the original cascade was decreased. At last, the original cascade and the combined slotted cascade were evaluated for aerodynamic performance, in detail, at the two blade solidities.

2. Cascade Models and Numerical Methods

2.1. Original Cascade and Combined Slotted Cascade

A high-turning compressor stator cascade was chosen as the original cascade, its camber angle is as large as 53.38°. Figure 1 shows the airfoil of the original cascade and one can see that its camber is more concentrated near the blade TE, which is typical of post-loaded blade profiles. Therefore, with the exception of the corner separation, the TE separation caused by the large camber is serious near the blade midspan when the inlet Mach number (Ma_1) is 0.7, which led to certain blade profile loss. Table 1 shows the main geometric and aerodynamic parameters of the original cascade and the blade-chord-based Reynolds number (Re_C) is 770,000 in simulation.

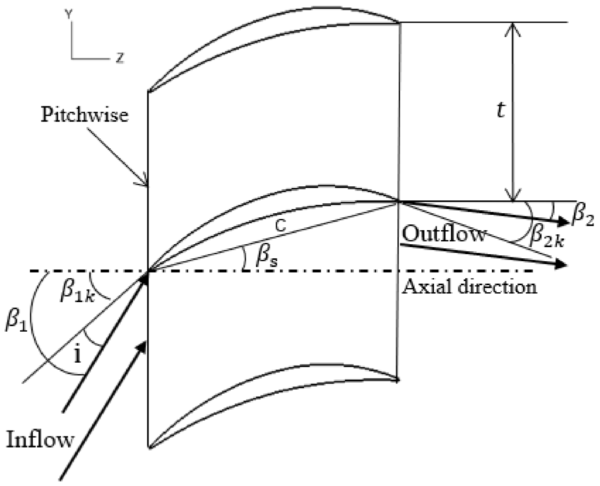

Figure 1. Airfoil of the original cascade.

Table 1. Main geometric and aerodynamic parameters of the original cascade.

Parameters	Values
Chord c/mm	63
Blade height H/mm	100
Aspect ratio H/c	1.59
Blade pitch t/mm	37.95
Blade solidity c/t	1.66
Stagger angle $\beta_S/(°)$	15.4
Geometric inlet angle $\beta_{1k}/(°)$	40.17
Geometric outlet angle $\beta_{2k}/(°)$	−13.21
Inlet Mach number Ma_1	0.7
Re_C	770,000

Figure 2a shows the overall configuration of the combined slotted cascade. According to the research of Zhou et al. [28], when the slot outlet is located before and relatively close to the separation point, the slot jet behaves and has a better control effect on separation. However, the blade TE separation and corner separation are both serious in the original cascade and the corner separation line (SL) is closer to the blade leading edge (LE) than the blade TE SL. Therefore, the full-span slot outlet was located at 75% of the blade axial chord (Ca) to comprehensively control the blade TE separation and the corner separation. In this case, the EW secondary flow will migrate on the blade SS before the full-span slot outlet, causing certain secondary flow loss. Hence, to control the development of the EW secondary flow, two blade-end slots were applied relatively near the blade LE. The blade-end slot occupies 10% of the blade height (H) and its outlet was set at 0.45 Ca.

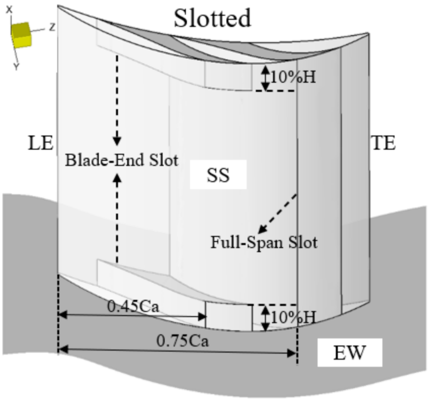

(**a**)

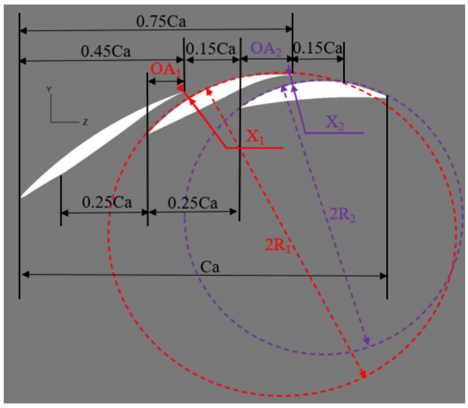

(**b**)

Figure 2. Combined slotted cascade: (**a**) overall combined slotted configuration (**b**) slot design parameters.

The design parameters of the full-span slot and blade-end slot are shown in Figure 2b. The inlet and outlet widths of the two slots were respectively set to 0.25 Ca and 0.15 Ca, thus the convergence of the slot passage ensures that the subsonic fluid can be effectively accelerated. In order to introduce the fluid of the blade pressure surface (PS) side into the slot without causing excess loss, the upper boundaries of the full-span and blade-end slots were set tangent to the blade PS [29]. Additionally, Denton's study [11] found that the mixing loss between the slot jet and the mainstream is closely related to the slot jet angle; the corresponding mixing loss increases with the increase in the slot jet angle. In this research, the slot jet angle is ensured through the tangential curved surface at the slot outlet and large axial overlap (OA). Hence, the OA_2 of the full-span slot and the OA_1 of the blade-end slot were set to be 0.1 Ca and 0.15 Ca, respectively, and the upper and lower boundaries of the two slots were set tangent with the blade SS.

In Figure 2b, X_1 and X_2 represents the outlet throat widths of the blade-end slot and full-span slot, respectively, while R_1 and R_2, respectively, represents the lower boundary outlet curve radiuses of the two slots. According to the Coanda effect [30], in order to ensure the slot jet flows along the slot lower boundary at the slot outlet without separation, the ratios of X_1/R_1 and X_2/R_2 were set to be a small value of 0.04. After the above settings, the mainstream of the blade PS side can be introduced into the full-span slot and blade-end slot and then it can be significantly accelerated. Meanwhile, the slot jet angle is the same as the mainstream direction of the blade SS side, which contributes to smaller mixing loss and effective re-energizing of low-momentum fluid.

2.2. Gird and Numerical Technique

Numerical simulations were conducted by Fine/Turbo of NUMECA international [31] in this research. The 3D RANS equations were solved in a single cascade passage with the use of periodicity boundary condition and the spatial discretization was based on a central difference format with second-order accuracy. Implicit residual smoothing method, multi-grid acceleration method and local time stepping method were adopted to accelerate the convergence of simulations. Additionally, the Spalart–Allmaras turbulence model [32] was used for the simulations.

The overall and partial simulation grids of the combined slotted cascade are shown in Figure 3 and the computational domain inlet boundary is 1.0c upstream away from the blade LE, while its outlet boundary is 2.0c downstream away from the blade TE. The structured multiblock grid was automatically generated for the original cascade by AutoGrid5 [33] of NUMECA international, which contains 3,000,000 grid points. In order to achieve a high grid quality, the "O4H-type" and "O-type" grid topologies were chosen to model the mainstream passage and around the blade, respectively. Non-slip adiabatic wall condition was set on the blade and EW. In addition, to capture the boundary layer and near-EW secondary flow, the grid size and density near the blade surface and the EW were refined. The minimum grid spacing on solid walls was set to be 5×10^{-6} m, which ensures the y^+ was smaller than 1.

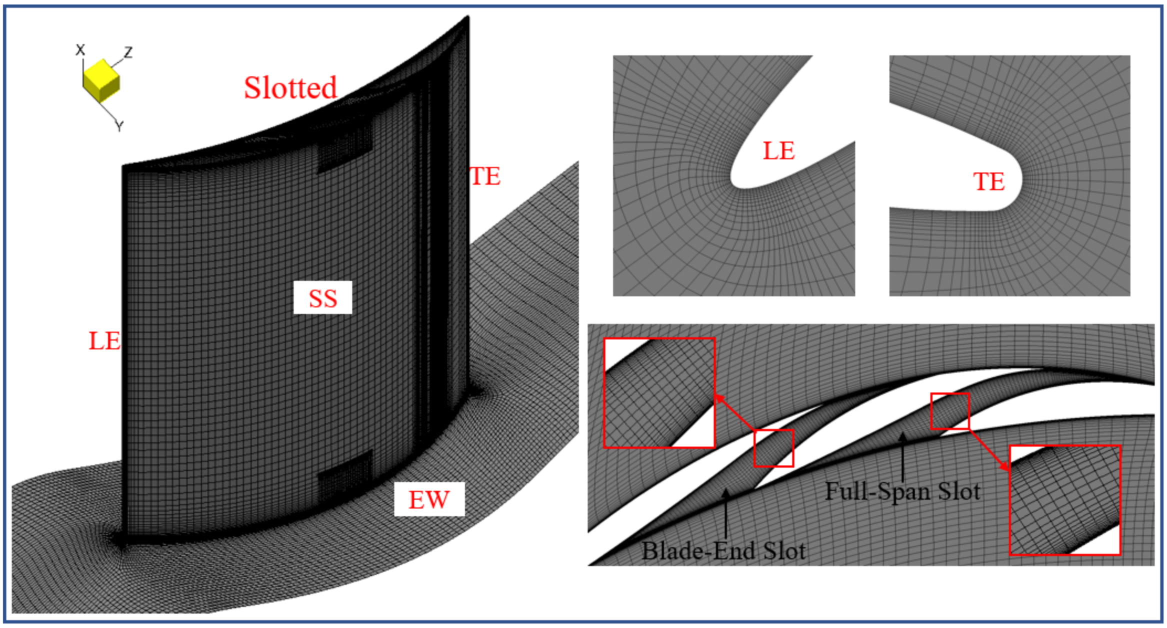

Figure 3. Overall and partial computational grid for the combined slotted cascade.

The "H-type" structured grid topology was applied in the full-span and blade-end slots, which was manually generated by IGG [34] of NUMECA international. The full-span slot grid and the blade-end slot grid, respectively, include 1,030,000 and 320,000 grid points. By using full non-matching connection technology, the slot grid and the cascade passage grid were connected to each other. The grid around the slot inlet and outlet were refined to ensure the correctness of the numerical value transfer during simulation. Moreover, the non-slip adiabatic wall condition was set on the upper and lower boundaries of the full-span and blade-end slots and the slot grid near the solid walls were then refined to capture the boundary layer in the slot.

At the computational domain inlet boundary, constant total pressure (101,325 Pa) and constant total temperature (288.15 K) were applied. The inlet incidence angle range and Mach number were, respectively, selected as $-6°$~$7°$ and a constant value of 0.7. The mass-flow was adjusted at the computational domain outlet boundary to ensure that the Mach number is fixed at 0.7. Increasing the blade pitch (t) from 37.95 mm to 46.32 mm, thus, the blade solidity was decreased from 1.66 to 1.36. At the two blade solidities of 1.66 and 1.36, the performance of the original cascade and combined slotted cascade was calculated. However, when the blade solidity is 1.36, $-6°$~$6°$ were selected as the inlet incidence angle range. Since the flow separation becomes serious with the decrease in solidity, it led to a rapid increase in total pressure loss under high incidence angles [26]. The SL moves toward the blade LE as the flow separation becomes serious and the slot outlet position should be changed to better control the flow separation [28]. Therefore, the outlet positions of the full-span and blade-end slots were set to be moved 0.05 Ca toward the blade LE at the blade solidity of 1.36. Additionally, the simulations were judged to be converged when the convergent mass-flow and the global mean residuals are less than 1×10^{-6}.

2.3. Simulation Results Validation

In order to verify the reliability of the numerical simulation method adopted in this research, firstly, the grid independence has been validated. In this research, the 3D mass-averaged aerodynamic parameters on the plane located 1.0c downstream from the blade TE were selected for overall performance parameters. For the datum cascade and the full-span slotted cascade, Figure 4 shows their total pressure loss coefficient variations with the increment of grid number under the incidence angle of 0°. Equation (1) shows the definition of the total pressure loss coefficient, p_{01} and p_1 present the inlet total pressure and static pressure, respectively, and p^* presents the local total pressure. One can observe from Figure 4 that the simulation results of the datum cascade tend to be converged when its grid number exceeds 3,000,000, while the simulation results of the full-span slotted cascade tend to be converged when the slot grid number exceeds 1,030,000, eliminating the influence of the grid number on the simulation results.

$$\omega = \frac{p_{01} - p^*}{p_{01} - p_1} \tag{1}$$

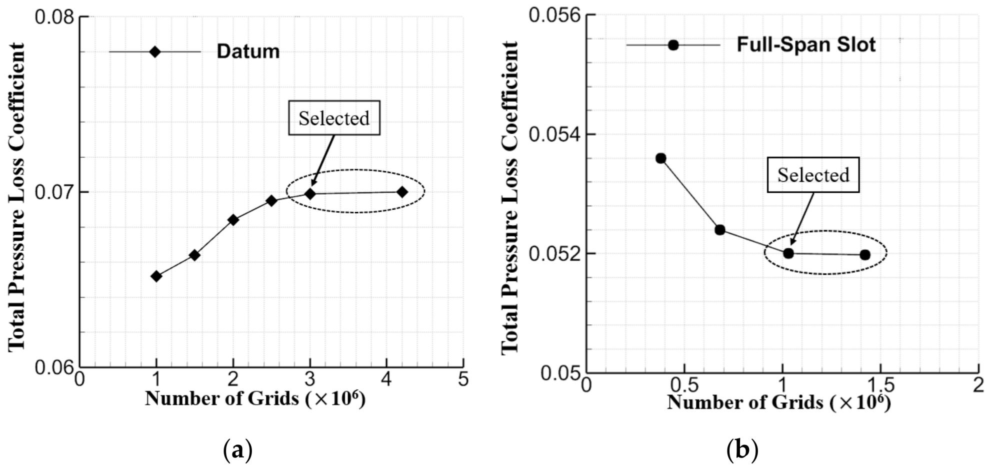

Figure 4. Grid independence validation: (**a**) datum cascade; (**b**) full-span slotted cascade.

Afterwards, the experiment of the original cascade was conducted when the inlet possessed Mach number of 0.6 and some experimental devices are shown in Figure 5. Figure 6 compares the blade surface static pressure coefficient of the simulation and experimental results at the midspan of the original cascade under the incidence angles of 0.5° and 5°. Equation (2) shows the definition of the static pressure coefficient, where p presents the local static pressure and p_{01} and p_1 are identical with the definition given for Equation (1). One can observe that the simulation results show good agreement with the experimental results under the two incidence angles and this verifies the credibility of the simulation results.

$$c_p = \frac{p - p_1}{p_{01} - p_1} \tag{2}$$

It is well known that the flow structure is complicated in the blade-end region and the simulation method should be further verified by the comparison of the simulation and experimental flow patterns in the blade-end region. Since there are no experimental flow patterns of the original cascade, another cascade denoted as the original_2 cascade [35] with relatively serious corner separation was used to further verify the reliability of the simulation method. The experimental and simulation flow patterns on the blade SS of the original_2 cascade are compared in Figure 7. The simulation flow patterns show excellent agreement with the experimental results, including the starting point (N) position of the SL, corner separation range and CSV. Therefore, the simulation method adopted in this research can simulate complicated flow patterns remarkably, which further proves that the simulation results in this research are reliable.

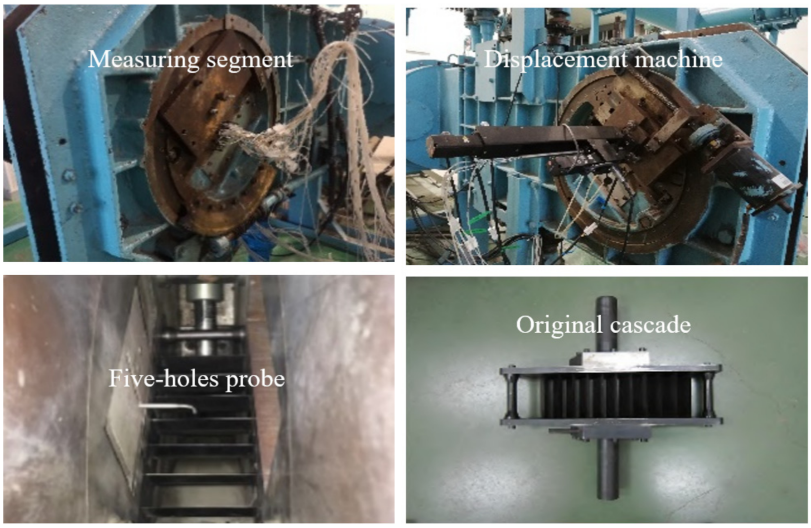

Figure 5. Some devices in the experiment of the original cascade.

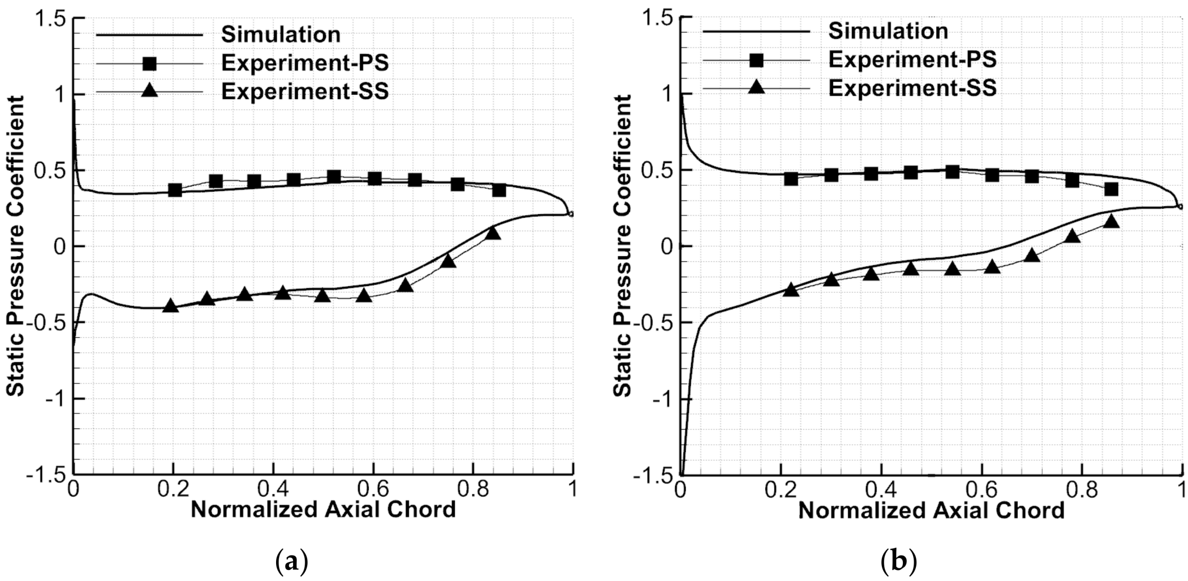

Figure 6. Comparison between the simulation and experimental results of the original cascade: (**a**) 0.5°; (**b**) 5°.

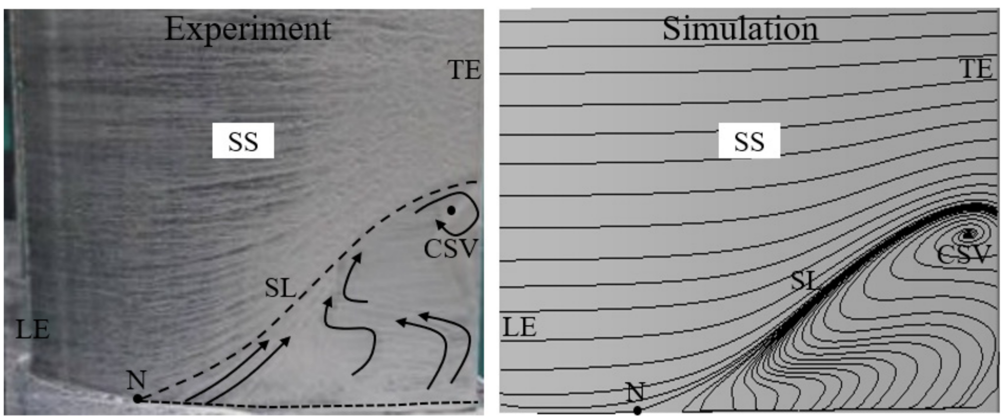

Figure 7. Experimental and simulation flow patterns on the blade SS of the original_2 cascade.

3. Results and Discussion

In this section, flow patterns and aerodynamic parameters were applied to evaluate the control effect of the combined slotted configuration on flow separation. In addition, due to the symmetry of the flow patterns of linear compressor cascade, the performance evaluation was conducted within 0–50% H to highlight the details of the flow patterns. At two blade solidities of 1.66 and 1.36, the performance of the original cascade and combined slotted cascade was compared in detail under two representative incidence angles of 0° and 6°. Afterwards, the overall performance of the two cascades was evaluated according to three aerodynamic parameters (total pressure loss, static pressure coefficient and turning angle) in the full incidence angle range.

3.1. Flow Patterns and Pressure Diffusing Capacity

Figure 8 shows the streamlines and velocity contours at 50% H and 5% H of the original cascade and combined slotted cascade under the incidence angle of 0° and 6°. One can see that with the decrease in the blade solidity from 1.66 to 1.36 and the flow separation becomes more serious at 50% H and 5% H under the incidence angle of 6°, while its degree does not change much under the incidence angle of 0°. The slot configuration designed in this research has a great self-adaptability to incidence angles. The fluid in the blade-end and full-span slots can be accelerated to the mainstream velocity of the blade SS side at the slot outlet under the two incidence angles, which ensures the significant re-energizing effect of the slot jet on the low-momentum fluid in the boundary layer. Therefore, the boundary layer profile separation and the corner vortex separation are both effectively eliminated in the combined slotted cascade at the blade solidities of 1.66 and 1.36. In addition, the combined slotted cascade has smaller mainstream velocity in the flow passage behind the blade TE compared to the original cascade. It can reflect that in comparison with that of the original cascade, the pressure diffusing capacity of the combined slotted cascade is improved. This is because in the combined slotted cascade, the elimination of the flow separation broadens the flow passage and increases the turning angle.

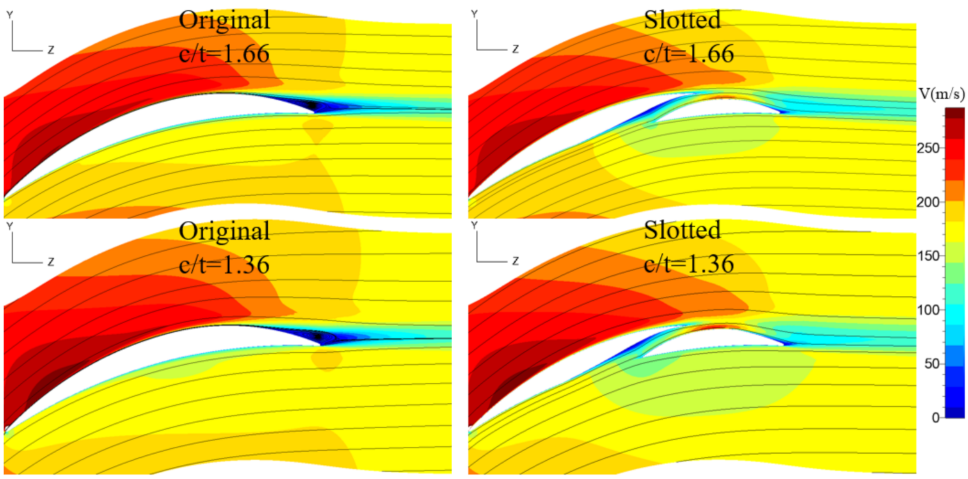

(**a**)

Figure 8. *Cont.*

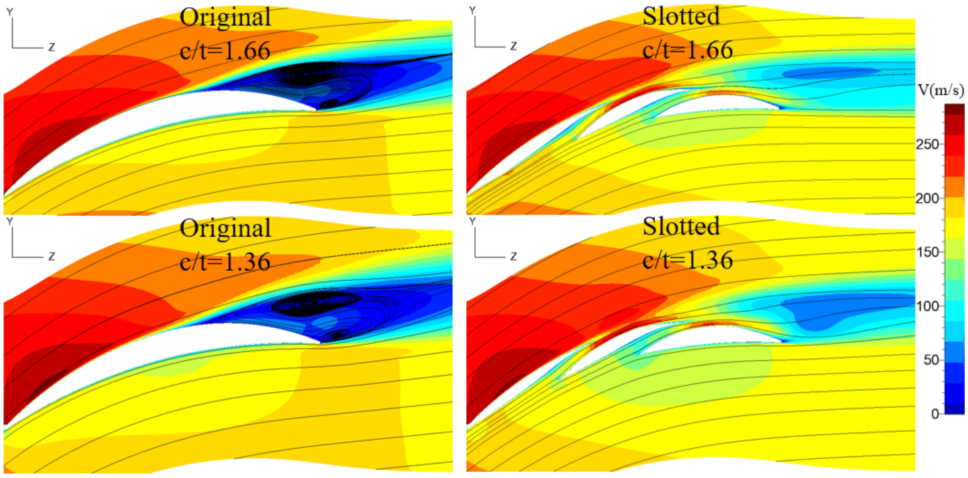

(**b**)

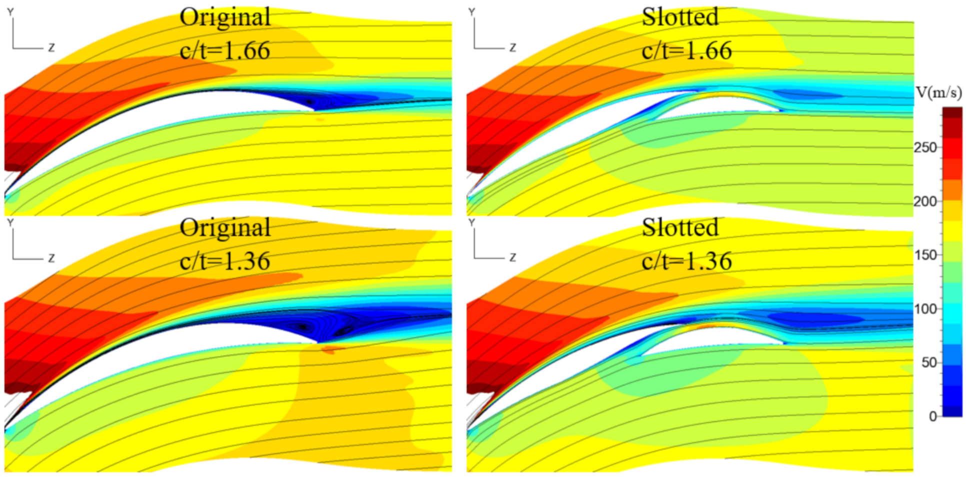

(**c**)

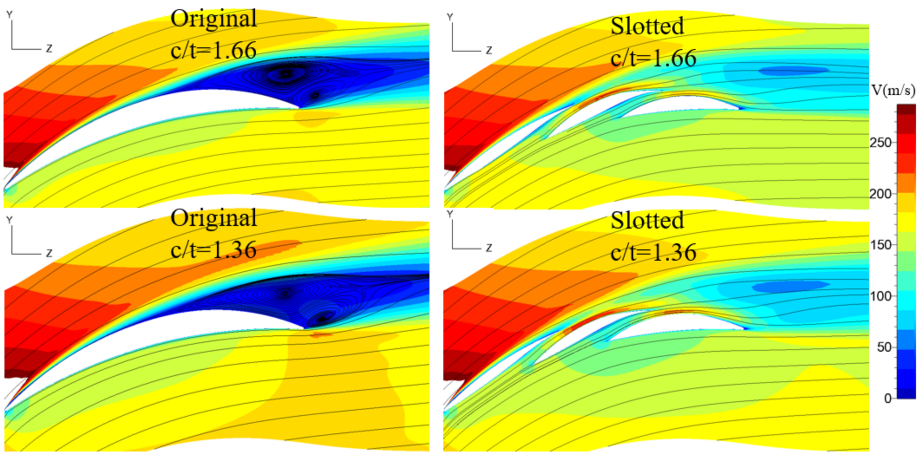

(**d**)

Figure 8. Streamlines and velocity contours of the original cascade and combined slotted cascade: (**a**) 0°—50%H; (**b**) 0°—5%H; (**c**) 6°—50%H; (**d**) 6°—5%H.

Figure 9a shows the limiting streamlines on the blade SS of the original cascade and combined slotted cascade under the incidence angle of 0°. Both the blade TE separation and corner separation exist in the original cascade. With the decrease in the blade solidity from

1.66 to 1.36, the starting point of the corner SL moves toward the blade LE and the corner separation range becomes larger. It is because of this that the decrease in the blade solidity leads to a higher pitch-wise pressure gradient, which transports more low-momentum fluid into the hub-corner region and, thus, enhances the corner separation. However, due to the blowing effect of the blade-end and full-span slots jets, the blade TE separation and corner separation are both controlled well in the combined slotted cascade at the two solidities. The blade-end slot jet plays an important role in control of the development of the EW secondary flow, contributing to a further reduction in the secondary flow loss.

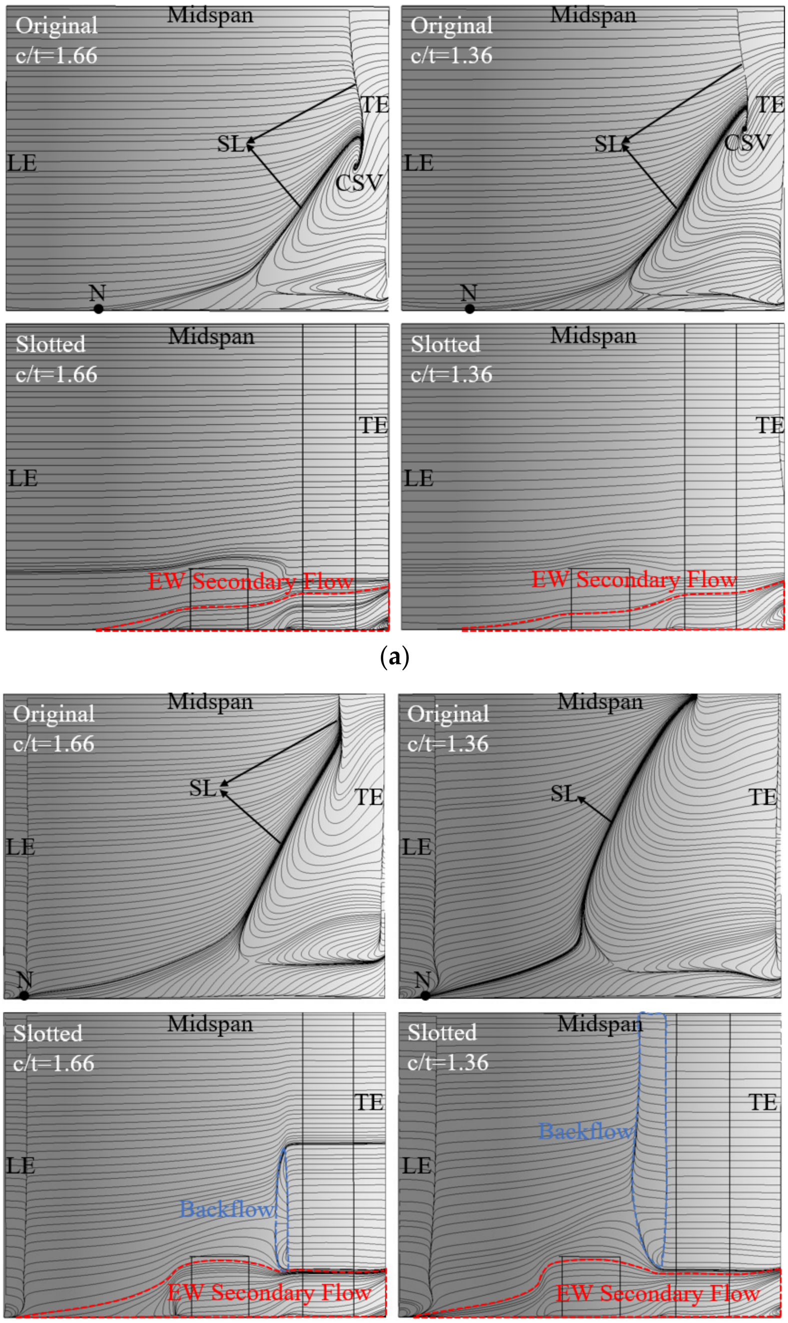

Figure 9. Limiting streamlines on the blade SS of the original cascade and combined slotted cascade: (**a**) 0°; (**b**) 6°.

Figure 9b shows the same contents as Figure 8a under the incidence angle of 6°. one can see that the corner separation becomes more serious in the original cascade as the incidence angle increases; the starting point of the corner SL moves to reach the blade LE. Moreover, the high incidence angle separates the incoming flow directly at the blade LE. However, the separated flow gradually adheres to the blade SS due to the mainstream action, which forms a blade LE separated bubble on the blade SS. Consistent with the situation of a 0° incidence angle, the corner separation becomes more serious in the original cascade under the incidence angle of 6° as the blade solidity decreases from 1.66 to 1.36. The corner separation occupies the whole blade span in the original cascade at the solidity of 1.36, which will cause serious passage blockage and loss. However, at the two blade solidities, the blade TE separation and corner separation are also well controlled in the combined slotted configuration under the incidence angle of 6°. The development of the EW secondary flow is suppressed under the combined blowing effect of the blade-end and full-span slots jets. Although the backflow zone caused by large adverse pressure gradient exists on the blade SS before the full-span slot outlet, the separated flow reattaches to the blade SS and flows to the blade TE without separation due to the full-span slot jet blowing effect.

In order to evaluate the impact of the combined slotted configuration on blade loading, Figure 10 shows the static pressure coefficient distributions on the blade surfaces of the original cascade and combined slotted cascade at different blade spans and incidence angles. One can see that with the decrease in the blade solidity from 1.66 to 1.36, the pressure difference between the blade PS and SS of the original cascade is enlarged, which reflects an increase in the blade loading. Moreover, the static pressure coefficient on the blade TE of the original cascade decreases due to the more serious flow separation, which is extremely obvious under the incidence angle of 6°. Hence, it can be concluded that under positive incidence angles, the decrease in the blade solidity leads to the decrease in the pressure diffusing capacity of the original cascade.

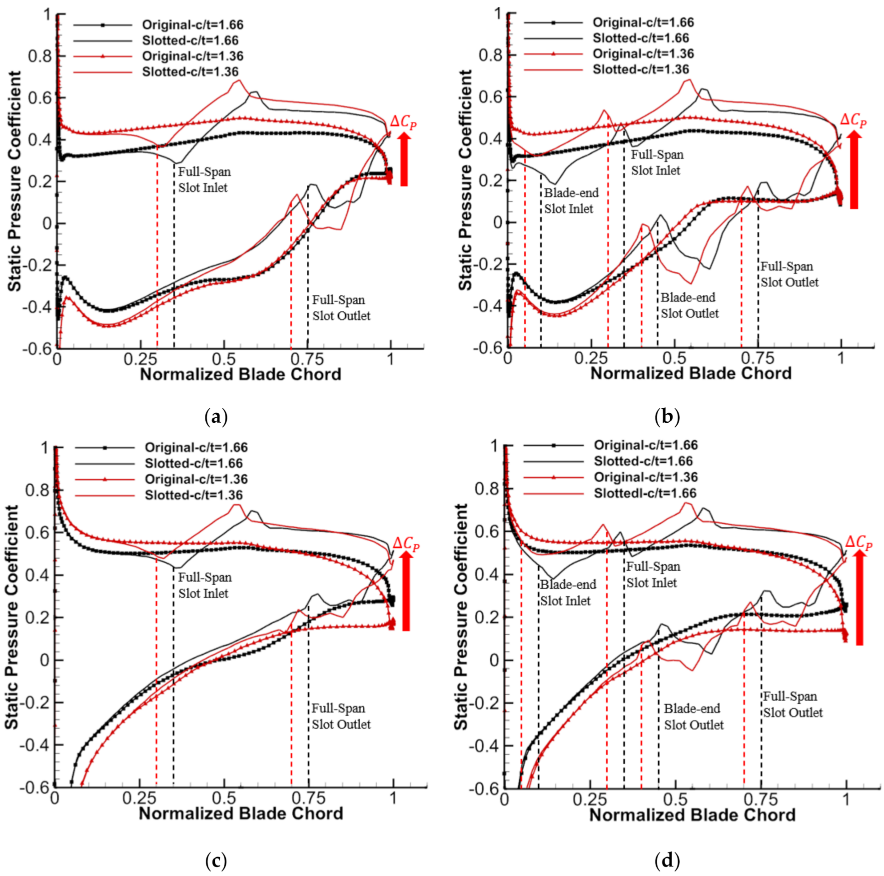

Figure 10. Static pressure coefficient distributions on the blade surfaces of the original cascade and combined slotted cascade: (**a**) 0°—50%H; (**b**) 0°—5%H; (**c**) 6°—50%H; (**d**) 6°—5%H.

According to the analysis of Figure 9, the elimination of the blade TE separation and the control of corner separation led to a significant improvement in the flow patterns of the combined slotted cascade. Therefore, the blade loading is increased behind the full-span slot outlet and the blade-end slot outlet at the two solidities. In addition, since the controlling of the flow separation broadens the flow passage and increases the turning angle, the blade TE static pressure coefficient of the combined slotted cascade is increased compared with that of the original cascade. That is, the combined slotted configuration can improve the pressure diffusing capacity of the original cascade remarkably. It can be found that the blade TE static pressure coefficient of the lower solidity combined slotted cascade is larger than that of the higher solidity original cascade, which means that the lower solidity combined slotted cascade has a stronger pressure diffusing capacity than the original higher solidity cascade. Hence, the combined slotted configuration has a certain potential in decreasing the single stage blade number for compressors, thus contributing to a decrease in compressor weight and an increase in aeroengine thrust-to-weight ratio.

In order to evaluate the impact of the combined slotted configuration on the vortex structures of the original cascade, Figure 11 shows the vortex structures in the flow passages of the original cascade and combined slotted cascade at the solidity of 1.66 under the incidence angles of 0° and 6°. Four cutting planes (S1, S2, S3 and S4) perpendicular to the z axis are shown in Figure 11 and their axial positions are 0.5 Ca, 0.75 Ca, 1.0 Ca and 1.25 Ca, respectively. The limiting streamlines on the four cutting planes and the volume streamlines in the cascade passage can effectively reflect the development of the vortex structures along the mainstream direction.

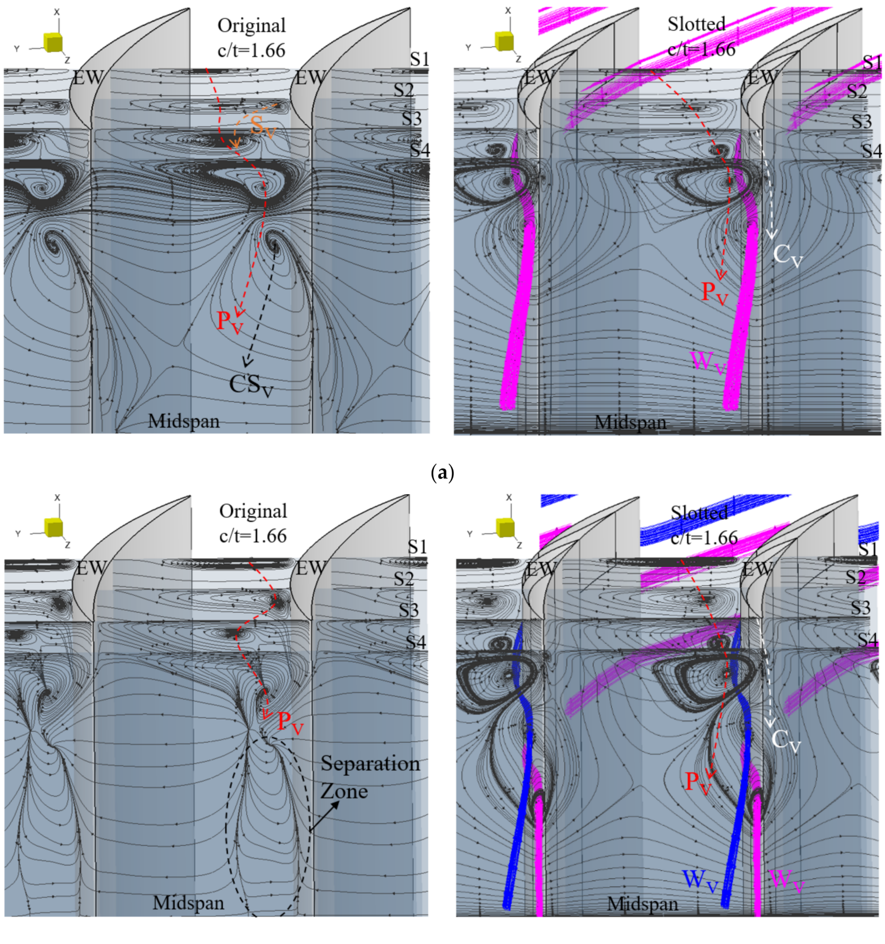

Figure 11. Vortex structures in the flow passages of the original cascade and combined slotted cascade at the solidity of 1.66: (**a**) 0°; (**b**) 6°.

Udner the incidence angle of 0°, there exists the separation vortex (S_V), P_V and CS_V in the original cascade passage, which is the main reason for the high loss corresponding to the corner separation. The S_V and P_V merge on the S3 cutting plane to form an enhanced P_V. Combined with the analysis of Figures 9 and 10, the S_V and CS_V is eliminated in the combined slotted cascade passage. However, under the higher adverse pressure gradient in the mainstream direction, the blade-end slot jet and the full-span slot jet interferes with one another and separates to form the wall vortex (W_V). The full-span slot jet and the near-EW flow also interferes with one another near the EW and separates to form the corner vortex (C_V). Additionally, the P_V is weakened in the combined slotted cascade passage. By observing the position of the P_V on the S3 cutting planes of the original cascade and combined slotted cascade, it can be found that the P_V is closer to the blade SS in the combined slotted cascade. This is because the reduction in the passage blockage and the higher blade loading causes the P_V to move toward the blade SS in the combined slotted cascade.

As the incidence angle increases from 0° to 6°, the P_V is enhanced and the CS_V is replaced by a large separation zone in the original cascade passage. Consistent with the situation of 0°, the P_V is weakened and it is closer to the blade SS in the combined slotted cascade, due to the higher blade loading and the reduction in the passage blockage. Under the remarkable combined blowing effect of the blade-end and full-span slots jets, the separation zone is eliminated in the combined slotted cascade under the incidence angle of 6°. However, the increase in the adverse pressure gradient in the mainstream direction leads to the generation of two W_V in the combined slotted cascade passage; one is formed by the separated mainstream and the other is formed by the separated full-span slot jet. In addition, the C_V is also generated in the combined slotted cascade passage due to the mutual interference of the full-span slot jet and the near-EW flow.

3.2. Loss and Turning Angle

In order to evaluate the effect of the combined configuration on the total pressure loss of the original cascade, Figure 12 shows the total pressure loss contours on the planes located 1.0c downstream from the blade TE of the original cascade and combined slotted cascade under the incidence angles of 0° and 6°. The high total pressure loss zone corresponding to the corner separation range is marked by the orange dotted box in Figure 12. One can observe that the corner separation range of the original cascade is enlarged under the two incidence angles as the blade solidity decreases from 1.66 to 1.36, which is consistent with the analysis of Figure 9. Combined with the analysis of Figure 11, although there exists the W_V and C_V in the combined slotted cascade passage, the W_V and C_V have smaller strength and range than the CS_V (or separation zone). Therefore, due to the weakening of the P_V and the elimination of the CS_V (or separation zone), the corner separation range is reduced in the combined slotted cascade.

In addition, at the blade solidity of 1.66, the combined slotted cascade has slightly larger total pressure loss near the blade midspan than the original cascade under the incidence angles of 0° and 6°. Since the TE separation near the blade midspan in the original cascade is relatively weak under the two incidence angles, the mixing of the full-span slot jet and the mainstream increases the wake loss development range. For the same reasons, when the blade solidity is 1.36, the total pressure loss near the blade midspan of the combined slotted cascade is slightly larger than that of the original cascade under the incidence angle of 0°. However, the corner separation occupies the whole blade span in the original cascade under the incidence angle of 6°, leading to higher total pressure loss near the blade midspan. In this case, the mixing of the full-span slot jet and the mainstream has slight effects on the development range of the wake loss. Therefore, due to the effective elimination of flow separation, the combined slotted cascade has a smaller total pressure near the blade midspan than the original cascade under the incidence angle of 6°. Taken as a whole, due to the significant reduction in the high total pressure loss caused by the corner separation, the combined slotted configuration can remarkably reduce the total pressure loss of the original cascade at different blade solidities and incidence angles.

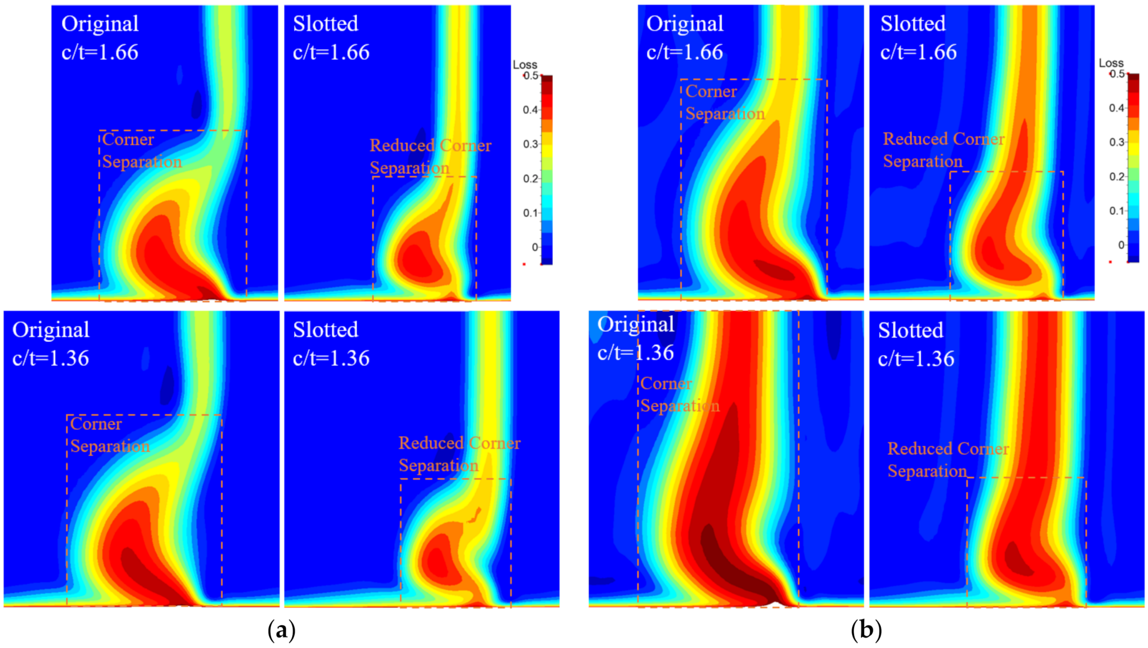

Figure 12. Total pressure loss contours on the planes located 1.0c downstream from the blade TE of the original cascade and combined slotted cascade: (**a**) 0°; (**b**) 6°.

Figure 13 shows the pitch-averaged turning angle distributions along the blade span on the planes located 1.0c downstream from the blade TE of the original cascade and combined slotted cascade under the incidence angles of 0° and 6°. The turning angle is defined in Equation (3), where β_1 and β_2 represent the inlet flow angle and outlet flow angle, respectively. Under the incidence angle of 0°, the turning angle of the original cascade is decreased as the blade solidity decreases from 1.66 to 1.36 because more serious flow separation brings a larger deviation angle. In the combined slotted cascade, the TE separation near the blade midspan is eliminated and the corner separation is well controlled at the two solidities. Therefore, the combined slotted cascade has a larger turning angle than the original cascade over the whole blade span. The improvement effect of the combined configuration on the turning angle of the original cascade is enhanced with the decrease in the blade solidity.

$$\Delta\beta = \beta_1 - \beta_2 \tag{3}$$

According to the analysis of Figure 9, the corner separation occupies the whole blade span in the original cascade under the incidence angle of 6° as the blade solidity decreases from 1.66 to 1.36. Hence, the turning angle of the original cascade is decreased with the decrease in the blade solidity under the incidence angle of 6° and the decreasing tendency is increased compared to the situation with a 0° incidence angle. However, the turning angle of the combined slotted cascade is still increased over the whole blade span at the two solidities compared with that of the original cascade, due to the effective control effect of the blade-end and full-span slots jets on the flow separation. Moreover, consistent with the situation of the 0° incidence angle, the combined slotted configuration has an enhanced improvement effect on the turning angle of the original cascade with the decrease in the blade solidity.

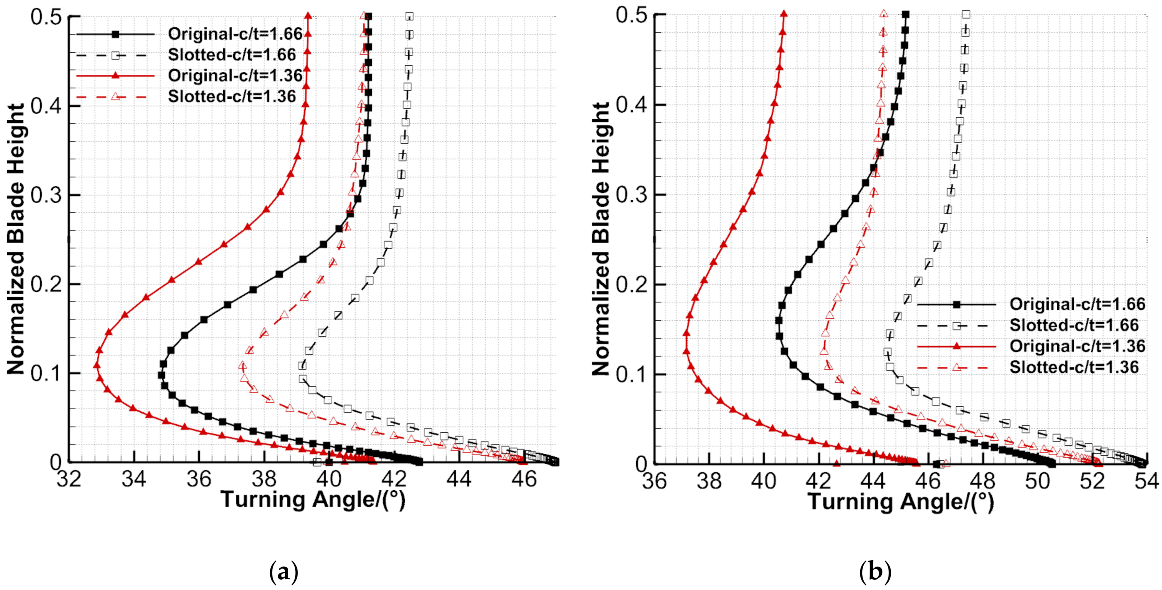

Figure 13. Pitch-averaged turning angle distributions along the blade span of the original cascade and combined slotted cascade: (**a**) 0°; (**b**) 6°.

3.3. Overall Performance

In order to evaluate the overall performance of the original cascade and combined slotted cascade, the aerodynamic parameters of the two cascades in the full incidence angle range are shown in Figure 14. Figure 14a shows the total pressure loss coefficient variation of the two cascades with the increment of incidence angle. The original cascade experiences more total pressure loss under positive incidence angles as the blade solidity decreases from 1.66 to 1.36, which is consistent with the study results of Sans et al. [26]. However, one can see that the combined slotted configuration can effectively control the flow separation in the full incidence angle range at the two solidities, thus the total pressure loss of the combined slotted cascade is decreased overall than when compared with that of the original cascade. When the blade solidity is 1.66, the total pressure loss can be decreased by an average of 23.2% in the combined slotted cascade and the maximum decrease is 28% under the incidence angle of 4°. When the blade solidity is 1.36, the total pressure loss can be decreased by an average of 27.7% in the combined slotted cascade, while the maximum decrease reaches 35.9% under the incidence angle of 4°. Therefore, it can be observed that the combined slotted configuration has an enhanced decreasing effect on the total pressure loss of the original cascade as the blade solidity decreases from 1.66 to 1.36. In addition, the total pressure loss difference between the original cascade and the combined slotted cascade is basically increased as the incidence angle increases. Hence, the combined slotted configuration also has an enhanced decreasing effect on the total pressure loss of the original cascade with the increase in the incidence angle.

Figure 14b shows the turning angle variation of the two cascades with the increment of incidence angle. The turning angle is increased within full incidence angle range in the combined slotted cascade; the average increase is 2.7° at the solidity of 1.66, while the average increase reaches 3.3° at the solidity of 1.36. Therefore, the combined slotted configuration has an enhanced improvement effect on the turning angle of the original cascade with the decrease in the blade solidity. Additionally, the improvement effect of the combined slotted configuration on the turning angle is also enhanced as incidence angle increases.

Figure 14c shows the static pressure coefficient variation of the two cascades with the increment of incidence angle. Since the effective controlling of the flow separation leads to a broadening of the flow passage and an increase in the turning angle at the blade solidities of 1.66 and 1.36, the combined slotted cascade possesses a larger static pressure coefficient in the full incidence angle range than compared with the original cascade. The static pressure coefficient can be increased by an average of 4.7% in the combined slotted cascade when the blade solidity is 1.66, while it can be increased by an average of 7.6% when the blade solidity is 1.36. Consistent with the variation trend of the turning angle, the combined slotted configuration has an enhanced improvement effect on the static pressure coefficient of the original cascade as the incidence angle increases or as the blade solidity decreases.

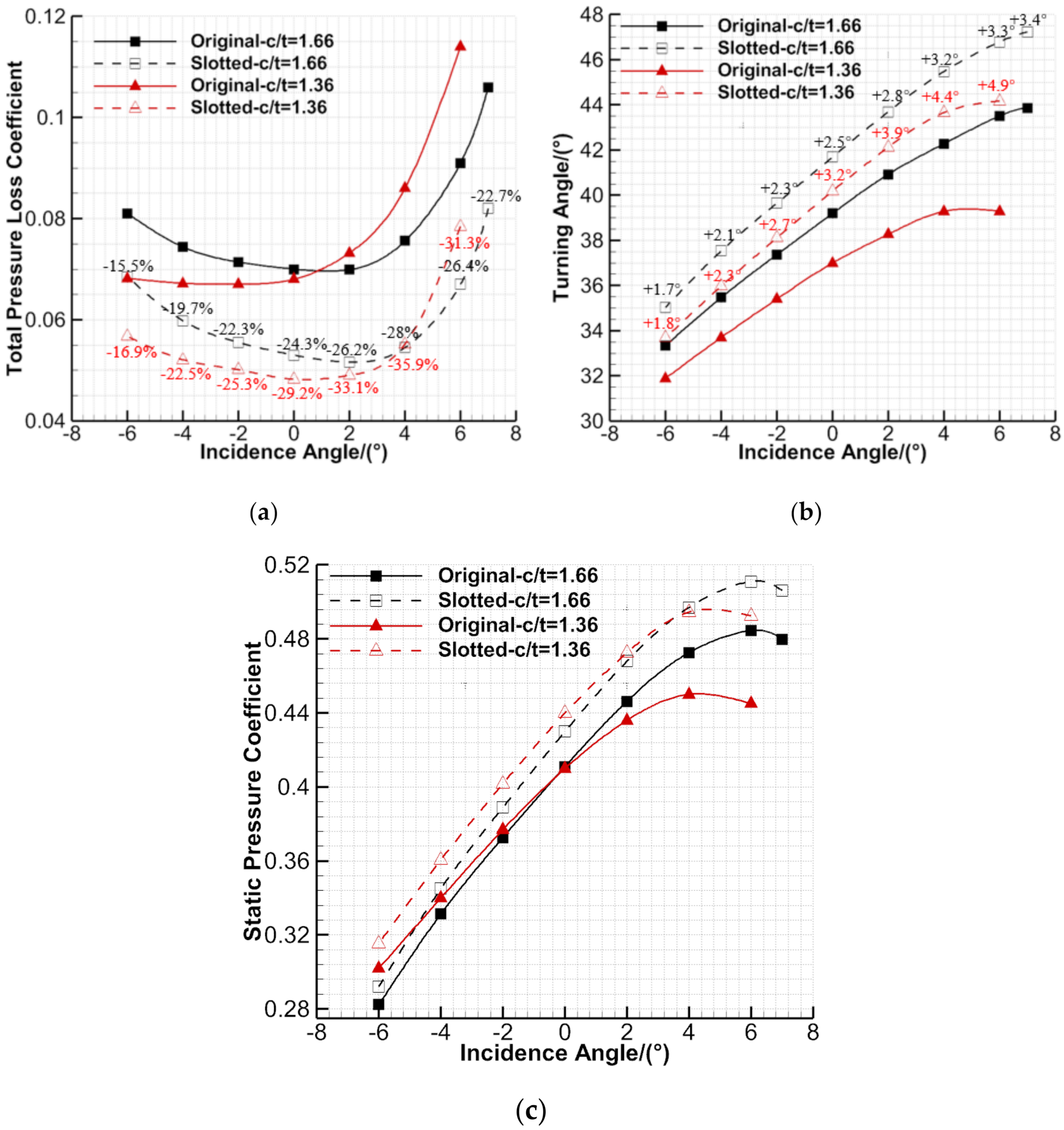

Figure 14. Aerodynamic parameters of the original cascade and combined slotted cascade in the full incidence angle range: (**a**) total pressure loss coefficient; (**b**) turning angle; (**c**) static pressure coefficient.

As a whole, the combined slotted configuration has a significant adaptability to the large separation or high loading conditions. This is because the combined slotted configuration has an enhanced control effect on the flow separation of the original cascade as the incidence angle increases or the blade solidity decreases. In addition, the lower solidity combined slotted cascade can achieve stronger pressure diffusing capacities than the higher solidity original cascade with smaller total pressure loss. Therefore, the combined slotted configuration shows a certain potential in decreasing the single stage blade number for compressors, thus contributing to a decrease in compressor weight and an increase in aeroengine thrust-to-weight ratio.

4. Conclusions

In order to effectively control the TE separation and corner separation in a high-turning compressor stator cascade, this research proposed a new combined slotted configuration consisting of one full-span slot and two blade-end slots. Meanwhile, to investigate the effect of the blade solidity on the combined slotted configuration, the performance of the original cascade and the combined slotted cascade was evaluated in a wide incidence angle range at two blade solidities. the following conclusions can be obtained:

1. The slot configuration designed in this research has a great self-adaptability to incidence angles. The fluid in the blade-end and full-span slots can be accelerated to the mainstream velocity of the blade SS side at the slot outlet under different incidence angles, which ensures the significant re-energizing effect of the slot jet on the low-momentum fluid in the boundary layer. Therefore, the flow separation can be controlled well in the combined slotted cascade within the full incidence angle range.
2. There exists the P_V and CS_V (or separation zone) in the original cascade passage, which is the main reason for its serious corner separation. Under the combined blowing effect of the blade-end and full-span slots jets, the P_V can be reduced and the CS_V can be effectively weakened in the combined slotted cascade. Thus, the corner separation is reduced remarkably in the combined slotted cascade, contributing to lower total pressure loss, higher turning angle and a broadening of the flow passage.
3. The corner separation range of the original cascade becomes larger as the blade solidity decreases from 1.66 to 1.36 under the incidence angles of 0° and 6°. However the development of the EW secondary flow before the full-span slot outlet can be effectively suppressed by the blade-end slot jet and when combined with the full-span slot jet blowing effect, the corner separation range can be reduced in the combined slotted cascade at the two blade solidities.
4. With the decrease in the blade solidity from 1.66 to 1.36, the blade loading and the blade TE static pressure coefficient of the original cascade are increased and decreased under the incidence angles of 0° and 6°, respectively. However, the slot jet significantly improves the flow patterns behind the slot outlet in the combined slotted cascade, hence its blade loading is increased behind the slot outlet at the two blade solidities compared with that of the original cascade and its blade TE static pressure coefficient is also increased remarkably.
5. The combined slotted configuration has a significant adaptability to the low blade solidity (or high loading) condition. By adopting the combined slotted configuration, the total pressure loss, turning angle and static pressure coefficient of the original cascade can be increased by −23.2%, 2.7° and 4.7 %, respectively, on average when the blade solidity is 1.66, while they can be increased by −27.7%, 3.3° and 7.6%, respectively, on average when the blade solidity is 1.36. Moreover, the lower solidity combined slotted cascade can achieve stronger pressure diffusing capacities than the higher solidity original cascade with smaller total pressure loss. Therefore, the combined slotted configuration shows a certain potential in increasing the aeroengine thrust-to-weight ratio by decreasing the compressor single-stage blade number.

Author Contributions: H.W. conducted the simulations and performed the analysis; Y.Q. and B.L. put forward the main idea and supervised the research work; H.W. and X.M. drafted the manuscript, discussed the results and reviewed the manuscript. All authors have read and agreed to the published version of the manuscript.

Funding: This research was funded by the National Natural Science Foundation of China (Project No: 51790512) and the National Major Science and Technology Projects of China (Project No: 2017-II-0001-0013).

Conflicts of Interest: The authors declare no conflict of interest.

Nomenclature

ω	Total pressure loss coefficient
c_p	Static pressure coefficient
p_{01}	Inlet total pressure
p^*	Local total pressure
p_1	Inlet static pressure
p	Local static pressure
$\Delta\beta$	Turning angle
β_1	Inlet flow angle
β_2	Outlet flow angle
β_{1k}	Geometric inlet angle
β_{2k}	Geometric outlet angle
β_s	Stagger angle
i	Incidence angle
c	Blade chord
Ca	Axial blade chord
H	Blade height
t	Blade pitch
Ma_1	Inlet Mach number
Re_C	Blade-chord-based Reynolds number
X_1	Blade-end slot outlet throat width
X_2	Full-span slot outlet throat width
R_1	Blade-end slot lower wall outlet curve radius
R_2	Full-span slot lower wall outlet curve radius
N	Starting point of the corner separation line

Abbreviations

EW	End-wall
PS	Pressure surface
SS	Suction surface
LE	Leading edge
TE	Trailing edge
CS_V	Concentrated shedding vortex
P_V	Passage vortex
S_V	Separation vortex
W_V	Wall vortex
C_V	Corner vortex
AO	Axial overlap
RANS	Reynolds Averaged Navier-Stokes
LES	Large-eddy simulation
DDES	Delayed detached eddy simulation

References

1. Wennerstrom, A.J. Highly loaded axial flow compressors: History and current developments. *J. Turbomach.* **1990**, *112*, 567–578. [CrossRef]
2. Wisler, D.C. Loss reduction in axial-flow compressors through low-speed model testing. *J. Eng. Gas Turbines Power* **1985**, *107*, 354–363. [CrossRef]
3. Li, R.Y.; Gao, L.M.; Ma, C.; Lin, S.Y.; Zhao, L. Corner separation dynamics in a high-speed compressor cascade based on detached-eddy simulation. *Aerosp. Sci. Technol.* **2020**, *99*, 105730. [CrossRef]
4. Gand, F.; Monnier, J.-C.; Deluc, J.-M.; Choffat, A. Experimental study of the corner flow separation on a simplified junction. *AIAA J.* **2015**, *53*, 1–9. [CrossRef]
5. Taylor, J.V.; Miller, R.J. Competing three-dimensional mechanisms in compressor flows. *J. Turbomach.* **2016**, *139*, 021009. [CrossRef]
6. He, C.; Ma, Y.F.; Liu, X.H.; Sun, D.K.; Sun, X.F. Aerodynamic instabilities of swept airfoil design in transonic axial-flow compressors. *AIAA J.* **2018**, *56*, 1–16. [CrossRef]
7. Gao, F.; Ma, W.; Zambonini, G.; Boudet, J.; Ottavy, X.; Lu, L.P.; Shao, L. Large-eddy simulation of 3-D corner separation in a linear compressor cascade. *Phys. Fluids* **2015**, *27*, 085105. [CrossRef]

8. Scillitoe, A.D.; Tucker, P.G.; Adami, P. Numerical investigation of three-dimensional separation in an axial flow compressor: The influence of freestream turbulence intensity and endwall boundary layer state. *J. Turbomach.* **2016**, *139*, 021011. [CrossRef]
9. Yan, H.; Liu, Y.W.; Li, Q.S.; Lu, L.P. Turbulence characteristics in corner separation in a highly loaded linear compressor cascade. *Aerosp. Sci. Technol.* **2018**, *75*, 139–154. [CrossRef]
10. Li, J.; Hu, J.; Zhang, C.K. Investigation of vortical structures and turbulence characteristics in corner separation in an axial compressor stator using DDES. *Energies* **2020**, *13*, 2123. [CrossRef]
11. Denton, J.D. Loss mechanisms in turbomachines. *J. Turbomach.* **1993**, *115*, 621–656. [CrossRef]
12. Cumpsty, N.A.; Greitzer, E.M. Ideas and methods of turbomachinery aerodynamics: A historical view. *J. Propuls. Power* **2004**, *20*, 15–26. [CrossRef]
13. MacMartin, D.G.; Tillman, T.G. Flow control opportunities in gas turbine engines. In Proceedings of the Fluids 2000 Conference and Exhibit, Proceedings of the Fluid Dynamics and Co-Located Conferences, Denver, CO, USA, 19–22 June 2000.
14. Ankit, S.; Francis, L. Topological studies of three-dimensional flows in a high pressure compressor stator blade row without and with boundary layer aspiration. *Chin. J. Aeronaut.* **2011**, *24*, 541–549.
15. Mao, X.C.; Liu, B.; Yuan, F.Z. Numerical and experimental study of separation control by boundary layer aspiration in a highly-loaded axial compressor cascade. *J. Appl. Fluid Mech.* **2018**, *11*, 433–446. [CrossRef]
16. Qin, Y.; Song, Y.P.; Chen, F.; Wang, R.Y.; Liu, H.P. Active flow control by means of endwall synthetic jet on a high-speed compressor stator cascade. *Proc. Inst. Mech. Eng. Part A J. Power Energy* **2017**, *232*, 641–659. [CrossRef]
17. Liu, H.P.; Yu, Y.C.; Chen, H.L.; Yu, M.H.; Zhang, D.F. A parametric investigation of endwall vortex generator jet on the secondary flow control for a high turning compressor cascade. *J. Therm. Sci. Technol.* **2017**, *12*, JTST0006. [CrossRef]
18. Zhao, W.F.; Zheng, Q.; Jiang, B.; Lin, A.Q. A passive control method of hub corner stall in a 1.5-stage axial compressor under low-speed conditions. *Energies* **2020**, *13*, 2691. [CrossRef]
19. Kan, X.X.; Wu, W.Y.; Yang, L.; Zhong, J.J. Effects of end-bend and curved blades on the flow field and loss of a compressor linear cascade in the design condition. *J. Therm. Sci.* **2019**, *28*, 801–810. [CrossRef]
20. Cao, Z.Y.; Liu, B.; Zhang, T.; Xu, Y.B.; Zhao, H. Non-axisymmetric endwall profiling in a highly loaded compressor cascade. *Proc. Inst. Mech. Eng. Part A J. Power Energy* **2018**, *233*, 275–292. [CrossRef]
21. Pan, R.C.; Song, Z.Y.; Liu, B. Optimization Design and Analysis of Supersonic Tandem Rotor Blades. *Energies* **2020**, *13*, 3228. [CrossRef]
22. Tang, Y.M.; Liu, Y.W.; Lu, L.P. Passive separation control with blade-end slots in a highly loaded compressor cascade. *AIAA J.* **2019**, *58*, 85–97. [CrossRef]
23. Hu, J.G.; Wang, R.G.; Huang, D.Q. Flow control mechanisms of a combined approach using blade slot and vortex generator in compressor cascade. *Aerosp. Sci. Technol.* **2018**, *78*, 320–331. [CrossRef]
24. Zweifel, O. The spacing of turbo-machine blading, especially with large angular deflection. *Brown Boveri Rev.* **1945**, *32*, 436–444.
25. Lieblein, S.; Schwenk, F.C.; Broderick, R.L. *Diffusion Factor for Estimating Losses and Limiting Blade Loadings in Axial-Flow-Compressor Blade Elements*; No. NACA-RM-E53D01; National Advisory Committee for Aeronautics, Lewis Flight Propulsion Lab: Cleveland, OH, USA, 1953.
26. Sans, J.; Resmini, M.; Brouckaert, J.F.; Hiernaux, S. Numerical investigation of the solidity effect on linear compressor cascades. In Proceedings of the ASME Turbo Expo 2014: Turbine Technical Conference and Exposition, Dusseldorf, Germany, 16–20 June 2014.
27. Tang, Y.M.; Liu, Y.W.; Lu, L.P. Solidity effect on corner separation and its control in a high-speed low aspect ratio compressor cascade. *Int. J. Mech. Sci.* **2018**, *142–143*, 304–321. [CrossRef]
28. Zhou, M.; Wang, R.G.; Cao, Z.H.; Zhang, X.Y. Effect of slot position and slot structure on performance of cascade. *Acta Aerodyn. Sin.* **2008**, *26*, 400–404. (In Chinese)
29. Sun, J.J.; Liu, Y.W.; Lu, L.P.; Xavier, O. Control of corner separation by slot at the root of the blade. *J. Eng. Thermophys.* **2019**, *40*, 2769–2776. (In Chinese)
30. Jones, G.S.; Viken, A.E.; Washburn, L.N.; Jenkins, L.N.; Cagle, C.M. An active flow circulation controlled flap concept for general aviation aircraft applications. In Proceedings of the 1st Flow Control Conference, St. Louis, MO, USA, 24–26 June 2002; AIAA Paper: Reston, VA, USA, 2002; p. 3157.
31. NUMECA International. *Fine/Turbo v8.7, User Manual*; NUMECA International: Brussels, Belgium, 2009.
32. Spalart, P.R.; Allmaras, S.R. A one-equation turbulence model for aerodynamic flows. In Proceedings of the 30th Aerospace Sciences Meeting and Exhibit, Reno, NV, USA, 6–9 January 1992; AIAA Paper: Reston, VA, USA, 1992; p. 439.
33. NUMECA International. *AutoGrid5 v8.7, User Manual*; NUMECA International: Brussels, Belgium, 2009.
34. NUMECA International. *IGG v8.7, User Manual*; NUMECA International: Brussels, Belgium, 2009.
35. Mao, X.C.; Liu, B.; Tang, T.Q. Effect of casing aspiration on the tip leakage flow in the axial flow compressor cascade. *Proc. Inst. Mech. Eng. Part A J. Power Energy* **2018**, *232*, 225–239. [CrossRef]